Hindawi
Journal of Engineering
Volume 2018, Article ID 7090524, 12 pages
https://doi.org/10.1155/2018/7090524

Research Article

Thermodynamic Analysis of a Solar Combined Ejector Absorption Cooling System

Doniazed Sioud, Raoudha Garma, and Ahmed Bellagi

Energy Engineering Department, Ecole Nationale d'Ingénieurs de Monastir (ENIM), University of Monastir, Tunisia

Correspondence should be addressed to Doniazed Sioud; siouddoniazed@gmail.com

Received 30 July 2018; Revised 15 October 2018; Accepted 24 October 2018; Published 11 November 2018

Academic Editor: Angelo Maiorino

The objective of this paper is to investigate theoretically a solar driven 60 kW absorption cooling system. The system is constituted of a combined ejector single-effect absorption cycle coupled with a linear Fresnel solar concentrator and using water/lithium bromide as working fluid. The combined ejector single-effect absorption cycle exhibits high performances, almost equal to that of double-effect absorption device. However, higher driving heat temperatures are required than in the case of conventional single-effect machines. A mathematical model is set up to analyze the optical performance of the linear Fresnel concentrator. Simulations are carried out to study the overall system performance COP_{system} and the performances of the combined absorption machine COP_{cycle} for generator driving temperatures and pressures in the ranges 180°C – 210°C and 198 kPa – 270 kPa, respectively. Further, the effect of operating parameters such as the cooling medium and chilled water temperatures is investigated. A maximum cycle performance of 1.03 is found for a generator pressure of 272 kPa and chilled and cooling water temperatures of 7°C and 25°C, respectively. A case study is investigated for a typical summer Tunisian day, from 8:00 to 18:00. The effect of ambient temperature and solar radiation on cycle and system performances is simulated. The optical performances of the concentrator are also analyzed. Simulation results show that between 11:00 and 14:00 the collector efficiency is 0.61 and that the COP_{cycle} reaches values always higher than 0.9 and the COP_{system} is larger than 0.55. Globally the performances of the investigated cycle are similar to those of double-effect conventional absorption system.

1. Introduction

In summer, the demand of electrical energy for air-conditioning and refrigeration becomes important, particularly in hot climate zones like the Mediterranean region. In many countries in this climate zone, the electric energy consumption reaches, and sometimes exceeds, in hot summer days the limit of production capacity. Consequently, the overall energy consumption and costs and the environmental impact become important. To reduce these impacts, solar cooling technologies may constitute a promising and attractive solution.

Solar energy applications and practices are investigated for different domains [1] such as pyrolysis [2], refrigeration and cooling [3], power generation [4], drying and various other industrial uses [5, 6]. In view of the increased interest in high temperature solar applications, many studies focus on the amelioration of collector configurations and concentrator techniques in order to improve their optical efficiency and the heat transfer characteristics of the absorber by using for instance nanofluids as a heat transfer fluids [7].

In the domain of refrigeration and air-conditioning, absorption techniques for production of cold are considered particularly suitable for solar applications. Single-effect absorption systems can be activated by flat plate collectors and/or evacuated tube collectors [8, 9] since they require relatively low temperatures of the driving heat sources. They have however low performances. Therefore, investigators focus attention on double-effect absorption cycles that need higher temperature heat sources provided by parabolic through collectors or linear Fresnel concentrators. Several investigations consider the technologies of double-effect absorption systems coupled with parabolic through collectors. An 11 kW solar absorption cooling system was studied by Florides *et al.* [10] in Nicosia and optimized using TRNSYS. The required parabolic collector area was 15m^2 and the capacity of hot

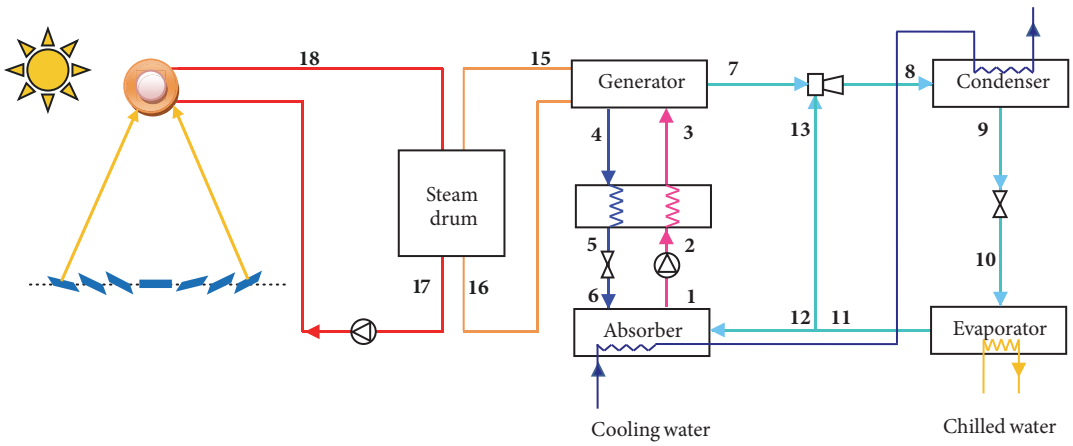

Figure 1: Solar combined ejector single-effect chiller.

water storage, 600 L. Shirazi *et al.* [11] investigated the feasibility of producing cooling via the connection of LiBr-H_2O single, double, and triple-effect absorption cycles to solar collectors under various weather conditions, namely, 1023 kW single-effect absorption chiller coupled with evacuated tube collectors (ETCs), parabolic trough collectors (PTC) coupled with 1163 kW double-effect and triple-effect units. The authors concluded that the energetic and economic performance of multieffect absorption machines coupled with concentrating collectors in low direct normal irradiation (DNI) fraction (less than 50%) climate zones is poor due to large solar field sizes required and high payback time compared to a single-effect chiller system driven by heat from evacuated tube collector array. On the other hand, in climatic regions with very high DNI faction (more than 65%), the combination of triple-effect chiller and parabolic trough collectors results in the most energy-efficient and cost-effective plant configuration, achieving the smallest solar field and the lowest payback period. Chemisana *et al.* [12] compared cooling systems connected and not connected to solar collectors. The solar cooling devices were basic single-effect absorption system that used heat from evacuated tube collectors, double-effect absorption system coupled with a Fresnel reflective collector incorporated on a building façade. These authors found that the solar absorber area of the Fresnel collector system was lower than that of standard solar thermal machine. Beltagy *et al.* [13] investigated theoretically and experimentally a solar cooling prototype with Fresnel collectors. The setup was designed basing on developed theoretical model, and experimental data was compared to numerical results. It was found that the measured and estimated produced thermal power from collectors and the efficiency per day were comparable. In addition, they found that the efficiency exceeds 40% per day for the 250 kW thermal prototype.

A 174 kW solar/gas double-effect LiBr/water absorption plant was tested at Seville in Spain [14]. The system was driven by a pressurized hot water flow using a 352 m^2 heated by a linear Fresnel collector. A direct-fired natural gas burner was used as auxiliary heat source. For 75% of generator's total heat input covered by solar energy, the average collector efficiency was found to vary between 0.35 and 0.4, and the mean coefficient of performance of the chiller, between 1.1 and 1.25.

Major drawbacks of the solar cooling systems are low efficiency in case of use of solar collectors with single-effect absorption systems and huge areas of thermal collectors required in case of double-effect absorption cycles. New machine configurations with high efficiency are needed. In literature, it is reported that some modified designs of single-effect chillers might exhibit coefficients of performance similar to that machines applying double-effect cycles [15, 16]. In these configurations, ejectors are incorporated in between generator and condenser.

The aim of this paper is to investigate a solar combined single-effect cycle using LiBr-H_2O as working fluid and coupled to solar collector. Because high temperature levels are needed to active the installation, a linear Fresnel collector is considered for the production of high temperature steam required to regenerate the refrigerant in the desorber. Driving temperature and chilled water temperature as well as cooling water temperature affect the performance of the chiller, COP_{cycle}, and the overall system performance, COP_{system}. Following simulations analyze thoroughly the effect of these three parameters. Also a case study of a typical Tunisian summer day is performed.

2. Description of the System

The proposed solar 60 kW cooling system is coupled with a 164 m^2 linear Fresnel collector, as schematically illustrated in Figure 1. The adopted collector (type IS-LF11 [17]) is used to produce steam at temperatures between 180°C and 230°C (pressures of 10 bar and 28 bar, respectively) for driving the generator of the combined cooling cycle. Cold is produced at temperatures between 12°C and 4°C.

The combined ejector single-effect cycle looks like an ordinary absorption single-effect cycle where an ejector is inserted between the generator and the condenser. The basic operational principle of the system is as follows: In the

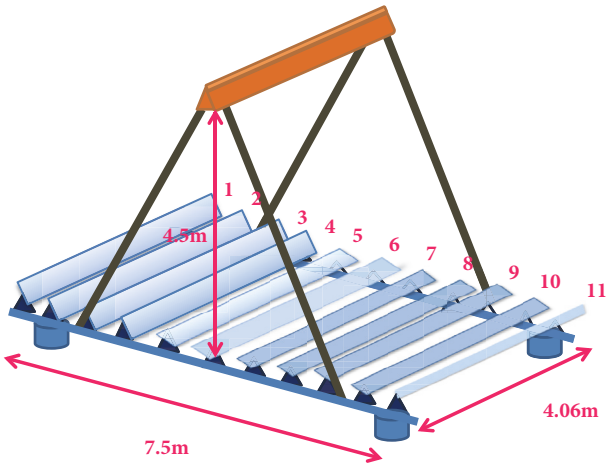

Figure 2: A module of industrial linear Fresnel collector.

Table 1: Technical data of basic IS-LF11 module [17]

Width (m)	7.5
Length (m)	4.06
Primary mirror area (m^2)	22
Receiver height (m)	4.5
Mirror rows number	11
Thermal loss of primary reflector, u_1 (W/m^2K^2)	0.00043
Clearance between mirror rows (m)	0-0.5
Specific weight (kg/m^2 installation surface area)	27
Maximum operational temperature (°C)	400
Life expectancy (years)	+20
Heat transfer flow	Pressurized Water or thermal oil

generator, the aqueous salt solution (H_2O/LiBr) is brought to boiling by heat provided by the solar source, in order to vaporize the refrigerant (water) and separate it from the solution. These high-pressure refrigerant vapors (7) are introduced in the ejector nozzle as primary flow where they are accelerated and strongly depressurized. A fraction of the vapor exiting the evaporator (13) is entrained by the primary flow into the ejector. The two gases are then well mixed in the mixing chamber and compressed in the diffuser (8) before feeding the condenser (9) where they liquefy by rejecting condensation heat to the cooling water (cw). The condensate expands through an adiabatic expansion valve (10) and proceeds to the evaporator where it evaporates (11) by absorbing heat from the chilled water. While in the basic cycle, all the refrigerant vapor leaving the evaporator proceeds to the absorber, only a part of it flows into the absorber in the combined cycle where it dissolves in the salt rich solution. The rest of the vapor is sucked in the ejector as secondary flow. The salt solution that leaves the absorber (1) is pumped to the generator (3), after preheating in the solution heat exchanger.

The generator is activated by the heat $\dot{Q}_g$ liberated by condensation of hot saturated steam (15) which is then pumped back as liquid (16) to the steam drum. A primary thermal transfer fluid loop (17-18) vehicles heat from solar collector to steam drum.

2.1. Solar Linear Fresnel Collector. IS-LF11 solar linear Fresnel collectors considered here are combined with boiler and can be used for industrial processes. Process heat in the range of 100 kW to 10 MW at standard pressure of 40 bar is generated, but up to 120 bar and temperatures up to 400°C are possible [17]. A "module" is one block of collectors associated with 4.06 m long vacuum absorber tubes. Figure 2 presents two modules of the adopted industrial collector. It is possible to use different kinds of heat transfer fluids (HTF): pressurized water, thermal oil, superheated steam, etc. Table 1 gives the manufacturer data of the commercial industrial Fresnel collector used in the simulations.

2.2. LiBr-H_2O Combined Ejector Single-Effect Absorption Chiller. In the investigated combined ejector single-effect absorption cycle the ejector is located between condenser and generator. It uses the vapor produced in the generator to entrain and compress the refrigerant vapor coming from the evaporator before flowing in the condenser. Consequently, the pressure in generator and condenser—equal in a conventional single-effect cycle—are now distinct: intermediate pressure in condenser, equal to the high pressure in the original cycle, and a higher pressure in the generator. Hence, higher driving source temperatures are now required, between 180°C and 210°C. Table 2 gives the assumed operating conditions in the simulations. In particular, the nominal cooling power of the installation is $\dot{Q}_e$ = 60 kW, available in form of chilled water at temperatures between 4°C and 12°C for driving temperatures and pressures in the range 180°C – 210°C and 198 kPa – 270 kPa, respectively.

2.3. Ejector. A typical ejector configuration is shown in Figure 3. A steam ejector is composed of four zones: primary nozzle, suction chamber, mixing chamber (convergent duct followed by constant section area), and diffuser. Table 3 gives the ejector geometrical data [16].

3. Theoretical Model

3.1. Linear Fresnel Collector Model. The optical efficiency $\eta_{optical}$ of the collector depends on the incidence angle of the direct irradiation. As reference of $\eta_{optical}$ is its value η_0 under ideal conditions: clean reflectors and absorber tubes, sun at zenith. For the adopted collector η_0 = 0.635 and η_{max} = 0.663 (sun at 5° transversal zenith angle, and 0° longitudinal zenith angle). For arbitrary incidence angle η_0 is multiplied by a correction factor, the so-called incidence angle modifier (IAM). IAM has two components: a field independent transversal component, IAM_t, and a longitudinal component, IAM_l, that depends on the number of in string assembled modules (one in Figure 2).

Table 2: Operating conditions assumed for the simulations.

Input parameter	Fixed value	Ranges
Capacity (kW)	60	
Generator temperature (°C)		180-210
Steam pressure (kPa)		198-270
Inlet temperature cooling medium (°C)	32	25-35
Chilled water outlet (°C)	7	7- 12
Heat exchanger efficiency	0.8	

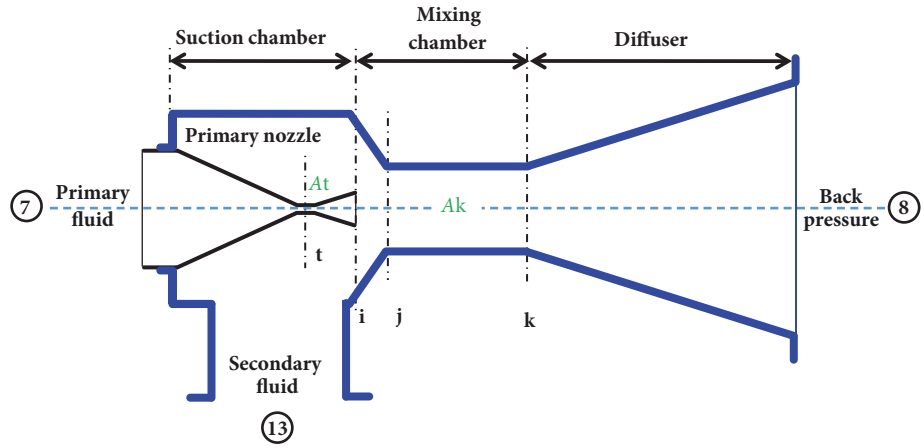

Figure 3: Schematic diagram of ejector.

Table 3: Ejector characteristics [16].

Parameter	Value
Nozzle throat diameter, d_t (mm)	1.6
Nozzle exit diameter, d_i (mm)	6
Mixing chamber diameter, d_j (mm)	18
Mixing chamber length (mm)	140
Diffuser divergent length (mm)	210
Diffuser exit diameter (mm)	40

The thermal losses of the reflector, $\dot{q}_{loss}$, are dominated by radiative losses and approximately estimated by

$$\dot{q}_{loss} = u_0 A_{aperture} \Delta T + u_1 A_{aperture} \Delta T^2 \quad (1)$$

$A_{aperture}$ stands for the active aperture area of the collector and ΔT for the temperature difference between that of the heat transfer flow HTF and the ambient, as expressed in

$$\Delta T = T_{HTF} - T_{amb} \quad (2)$$

The thermal loss coefficients of the IS-LF11 are $u_0 = 0$ and $u_1 = 43.\ 10^{-5}\ \mathrm{W/m^2K^2}$ [17]. Equation (1) reduces then to

$$\dot{q}_{loss} = 43.10^{-5} A_{aperture} \Delta T^2 \quad (3)$$

The collected thermal power $\dot{q}$ writes as

$$\begin{aligned} \dot{q} &= \eta_{optical} AG - \dot{q}_{loss} \\ &= \eta_0 IAM_l(\theta_{l,\delta})\, IAM_t(\theta_{t,\delta})\, A_{aperture} G \\ &\quad - u_1 A_{aperture} \Delta T^2 \end{aligned} \quad (4)$$

where θ is the zenith angle, δ, the angle between absorber pipe and the north-south direction, and G, the direct normal irradiance (DNI).

The thermal efficiency of the collector η is the ratio of the usable thermal power $\dot{q}$ and the solar irradiance collected ($A_{aperture}G$), detailed in

$$\begin{aligned} \eta &= \frac{\dot{q}}{A_{aperture}G} = \eta_{optical} - \frac{\dot{q}_{loss}}{A_{aperture}G} \\ &= \eta_0 IAM_l(\theta_{l,\delta})\, IAM_t(\theta_{t,\delta}) - u_1 A_{aperture} \frac{\Delta T^2}{G} \end{aligned} \quad (5)$$

Figure 4 depicts this correlation, η *versus*$(\Delta T/G)$, for the adopted collector and various values of G [17]. It is worthy noticing that knowing thermal efficiency, irradiation, and actual collector size, the expected gross heat produced by the collector can be predicted.

3.2. Combined Ejector Single-Effect Absorption Cycle Model. The mathematical model of the cycle is based on mass and energy balances written for each machine element. For a steady state process and neglecting kinetic and potential

Table 4: Comparison of results from [16] with those of present work.

	Ref. [16]	Present work
Condenser pressure (kPa)	< 3	3.78
Generator temperature (°C)	192	192
Generator Pressure (°C)	198	198
Concentration at absorber exit (mass. %)	62.3	62.3
Refrigerant mass flow rate, generator (kg/min)	0.0393	0.0393
Refrigerant mass flow rate, evaporator (kg/min)	0.059	0.063
$\dot{Q}_g$(kW)	2.8	2.8
$\dot{Q}_e$(kW)	2.4	2.5
COP	0.87	0.91

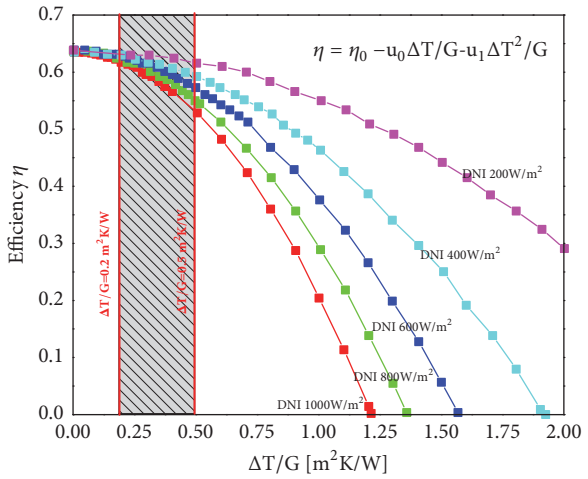

Figure 4: Collector thermal efficiency η *versus* $(\Delta T/G)$ for various values of G.

energy variations, balance equations for global mass (equation (6)), salt mass (equation (7)), and energy (equation (8)) write, respectively,

$$\sum \dot{m}_{in} = \sum \dot{m}_{out} \tag{6}$$

$$\sum \dot{m}_{in} X_{in} = \sum \dot{m}_{out} X_{out} \tag{7}$$

$$\sum \dot{Q} - \sum \dot{W} = \sum \dot{m}_{out} h_{out} - \sum \dot{m}_{in} h_{in} \tag{8}$$

$\dot{Q}$ and $\dot{W}$ are heat and transfer rates between machine element and its surroundings. The COP_{cycle} of the absorption system is expressed as

$$COP_{\text{cycle}} = \frac{\dot{Q}_e}{\dot{Q}_g + \sum \dot{W}_{\text{P}}} \tag{9}$$

3.3. Ejector Model. The adopted 1D model of the ejector is detailed in reference [15]. It is based on quadratic equations of each zone and enables the prediction of the ejector performance, i.e., the entrainment ratio (ratio of mass flow rate of the primary flow $\dot{m}_7$ and secondary flow rate $\dot{m}_{13}$) for given ejector geometry and inlet and outlet pressures and temperatures.

4. Validations

A computer programs are developed using the software Engineering Equation Solver (*EES*) [20] in order to validate thermodynamically the models of combined ejector single-effect absorption unit and steam ejector.

4.1. Validation of Combined Ejector Single-Effect Model. The simulations are run under following conditions, according to the data of [16]:

(i) Evaporator temperature: 5∘C

(ii) Condenser temperature: 28∘C

(iii) Concentrations of salt solution leaving absorber: 62.3%

(iv) Heat exchanger effectiveness: 0.8

(v) Solution flow rate leaving generator: 0.393 kg/min

(vi) Generator pressure: 198 kPa and temperature: 192∘C

Table 4 compares the obtained simulations results with those reported by Aphornratana *et al.* [16]. As can be noted, deviations are generally small, less than 1%, with a maximum of 6% for the mass flow rate of refrigerant leaving the evaporator. This can be attributed to the simplifying assumption of perfect gas behavior for the steam in the ejector model. Deviations of driving power and cooling load are respectively 0.3% and 6%. Thus, the proposed model for the simulation of the chiller is fairly validated.

4.2. Validation of Ejector Model. In the experimental work of Sriveerakul *et al.* [19], various combinations of ejector geometry were tested for different operating temperatures and pressures. Primary and secondary flows were vapors. The 1D model used for the machine simulations is tested against the data of this experimental work for validation. Calculated results are compared with data reported in [19] in Table 5.

Deviations ε% for backpressure, entrainment ratio, and ejector area ratio are determined as

$$\varepsilon\% = \frac{\text{calculated value} - \text{experimental value}}{\text{experimental value}} \tag{10}$$

Minimum absolute percent deviation of backpressure is 3% and maximum, 23%. For entrainment ratio the corresponding values are 0.3% and 18%, and for ejector area ratio, 0% and

Table 5: Ejector model validation (T_p, primary flow temperature;T_s, entrained flow temperature; (A_k/A_t), ejector area ratio, *i.e.,* ratio of constant area section, A_k, and nozzle throat area, A_t).

Backpressure (mbar)			Entrainment ratio			(A_k/A_t)		
Exp. [19]	Cal.	ε (%)	Exp. [19]	Cal.	ε (%)	Exp. [19]	Cal.	ε (%)
$T_p = 120^\circ$C, $T_s = 10^\circ$C								
0.53	0.48	-10.	90.25	103	14.	37	37	0
$T_p = 130^\circ$C, $T_s = 10^\circ$C								
0.4	0.39	-3.	90.25	97.71	18.	50	50	0
$T_p = 140^\circ$C, $T_s = 15^\circ$C								
0.28	0.33	18.	90.25	96.02	6.	65	65	0
$T_p = 130^\circ$C, $T_s = 5^\circ$C								
0.31	0.32	5.	90.25	96.55	7.	48	48	0
0.39	0.43	13.	117.9	117.5	-0.3	41	37	11.
0.47	0. 57	23.	160.5	144.2	-10.	35	31	13.
0.31	0.36	19.	90.25	104.6	16.	45	43	5.
0.3	0.35	18.	90.25	101.7	13.	46	46	0

13%. Based on the simulation results and percent deviations reported in Table 5, it can be concluded that the proposed 1D ejector model describes fairly well the experimental data.

5. Solar Chiller Simulation Results and Discussion

Simulations of a 60 kW solar chiller are performed in order to analyze thermodynamically and predict the performances of a combined ejector single-effect absorption refrigeration cycle coupled with linear Fresnel collector modules. The computer program was developed using the software Engineering Equation Solver (*EES*) [20]. Thermophysical properties of the refrigerant system LiBr-H_2O are determined by applying internal procedures of the software. Tunisian climate and meteorological data are taken into consideration in the program.

A solar absorption chiller is characterized by an overall coefficient of performance, COP_{system}, a key factor to describe the efficiency of the entire system, expressed in (11), and is defined as the product of the efficiency of the solar collector η and the thermal coefficient of performance of the absorption refrigerant cycle COP_{cycle} [21]:

$$COP_{system} = \eta COP_{cycle} \quad (11)$$

5.1. Effect of Generator Temperature and Pressure on System Performance (for Constant Chilled Water Temperature). Simulations are performed by varying gene rotor temperature and pressure as well as the cooling medium temperature, for fixed chilled outlet-temperature, $T_c = 7^\circ$C. The results are represented graphically in Figures 5(a), 5(b) and 5(c), for, respectively, three values of the generator pressure 198 kPa, 232 kPa, and 272 kPa. The coefficient of performance of the chiller COP_{cycle} together with the performance of the whole installation COP_{system}, including the solar facility, is depicted *versus* generator temperature for three values of the generator pressure and cooling medium temperature.

Table 6: Maximum *COP* reached for solution generator temperature set at 210°C (maximum considered) and $T_c = 7^\circ$C.

$P_{generator}$ (kPa)	COP_{system}	COP_{cycle}	T_{cw} (°C)
198	0.57	0.99	25
	0.52	0.85	30
	0.46	0.75	35
232	0.59	1.02	25
	0.53	0.88	30
	0.47	0.77	35
270	0.6	1.03	25
	0.54	0.89	30
	0.48	0.79	35

Given these findings, we note that

(i) The *COP* increases with increasing generator temperature, T_g. For fixed T_g, it decreases with decreasing cooling water temperature.

(ii) The COP_{cycle} reaches values ranging from 0.4 to 1.03, reaching the performances of double- effect absorption cycles, thus larger than what can be obtained in case conventional single-effect without ejector [22].

(iii) The COP_{system} is almost half COP_{cycle} due to the limited efficiency of the solar collector installation. Even in the case of favorable conditions, in gray high-lightened zone in Figure 4 and representing a common situation in Tunisian summer, this efficiency is ranging between 0.5 and 0.6.

(iv) It is observed that the maximum COP_{cycle} (and consequently the COP_{system}) attains higher values when the generator pressure is larger. The highest performances are reached for the maximum generator temperature considered in this study, $T_{g,max} = 210\circ$C. Table 6 summarizes these results. In fact, for minimal cooling medium temperature (25∘C) and highest generator temperature (210∘C), the $COP_{cycle} = 0.99, 1.02, 1.03$

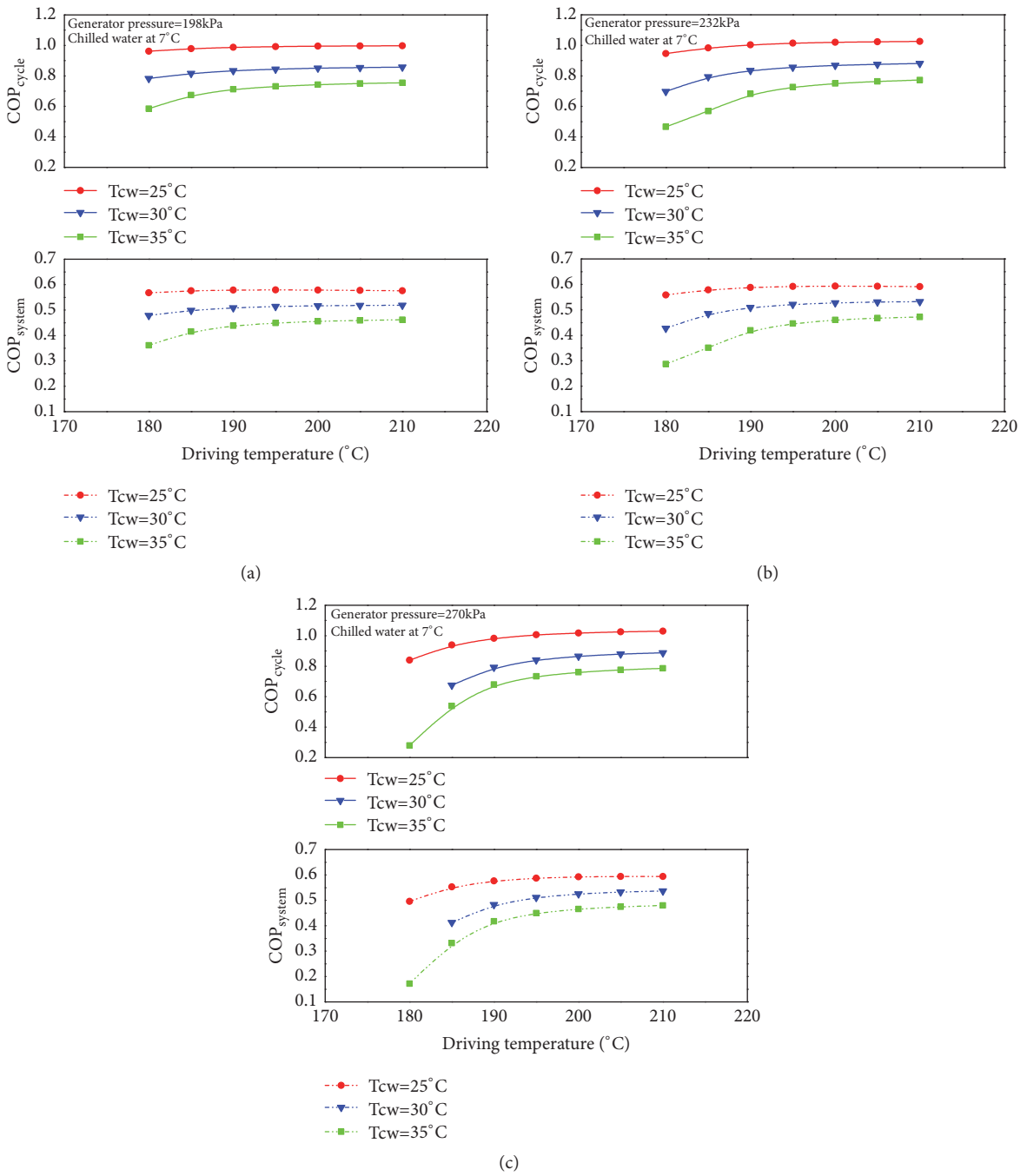

Figure 5: Effect of generator temperature on system performance for different generator pressures and cooling medium temperatures.

and the COP_{system} = 0.57, 0.59, 0.6 for generator pressures at 198 kPa, 232 kPa, 272 kPa, respectively. It is noticed further that

(v) For a fixed generator pressure, the maximum *COP* decreases when the temperature of the cooling medium rises. So when the pressure in the generator is at 198 kPa, the maximum COP_{cycle} = 0.99, 0.85, 0.75 for cooling medium temperature, respectively, set at 25∘C, 30∘C, 35∘C, with the corresponding values for COP_{system} = 0.57, 0.52, 0.46.

(vi) The performances of cycle and system are optimal for the highest generator pressure (270 kPa), lowest cooling medium temperature (25∘C), and largest chilled water temperature (12∘C).

5.2. Effect of Generator Temperature and Pressure on System Performance (for Constant Cooling Medium Temperature). Similar simulations are run by maintaining constant the cooling medium temperature T_{cw} = 32°C and varying the chilled water temperature T_c. Figures 6(a), 6(b) and 6(c) present the evolution of COP_{cycle} and COP_{system} of the solar

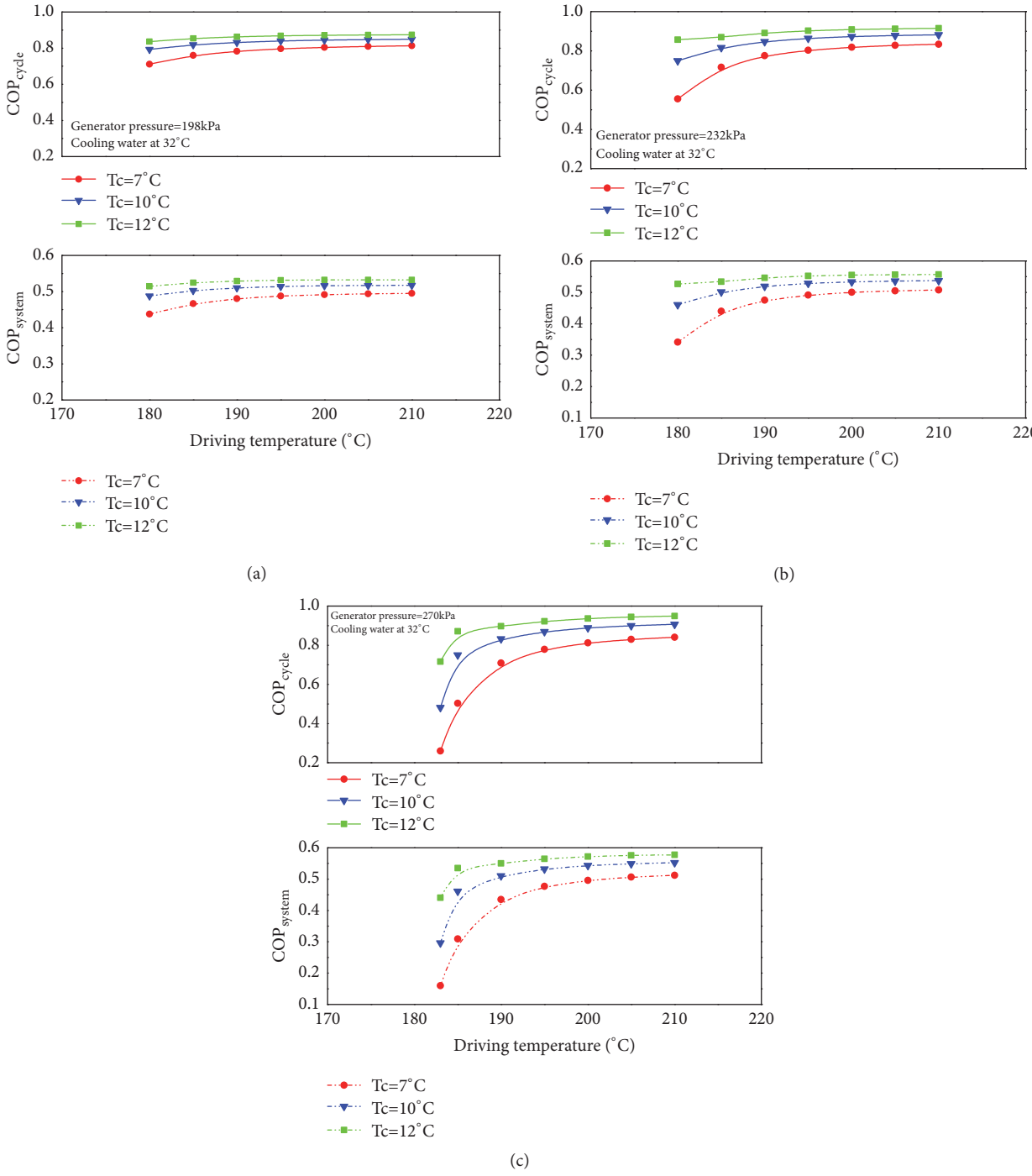

Figure 6: Effect of generator temperature on system performance for different generator pressures and chilled water temperatures.

combined single-effect absorption refrigeration system for three values of the generator pressure 198 kPa, 232 kPa, and 272 kPa, respectively. It can be noted that

(i) Again, both COP_{cycle} and COP_{system} increase when the generator temperature is increased.

(ii) COP_{cycle} and COP_{system} increase with the driving temperature, similarly to the behavior already observed in Figure 5. Table 7 gives the maximum of cycle and system performances, when the driving temperature reaches its highest value, 210∘C. For T_c = 12∘C COP_{cycle} reaches 0.87, 0.91, and 0.95 for generator pressure 198 kPa, 232 kPa, and 270 kPa, respectively.

(iii) The performances of cycle and system (COP_{cycle} and the COP_{system}) increase with increasing chilled water temperature. For example, as shown in Table 7, for generator pressure equal to 270 kPa, the maximum

Table 7: Maximum *COP* reached for solution generator temperature set at 210°C (maximum considered) and T_{cw} = 32°C.

$P_{generator}$(kPa)	COP_{system}	COP_{cycle}	T_c (°C)
198	0.50	0.81	7
	0.52	0.85	10
	0.53	0.87	12
232	0.51	0.83	7
	0.54	0.88	10
	0.56	0.91	12
272	0.51	0.84	7
	0.55	0.91	10
	0.58	0.95	12

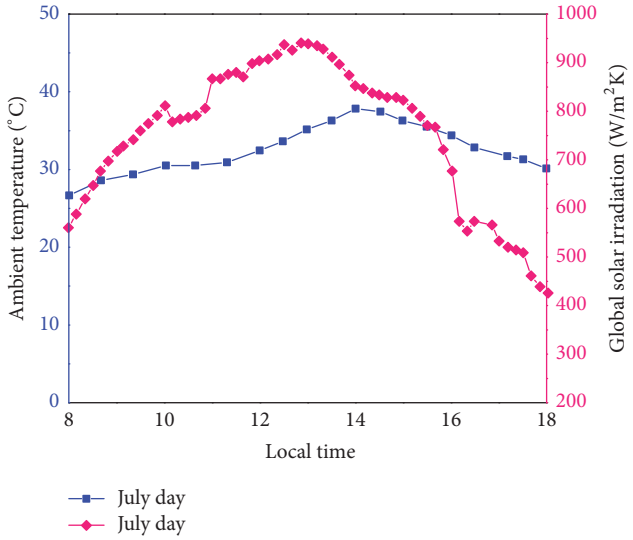

Figure 7: Evolution of solar radiation and ambient temperature in a typical summer day (July 16) in Tunis-Tunisia [18].

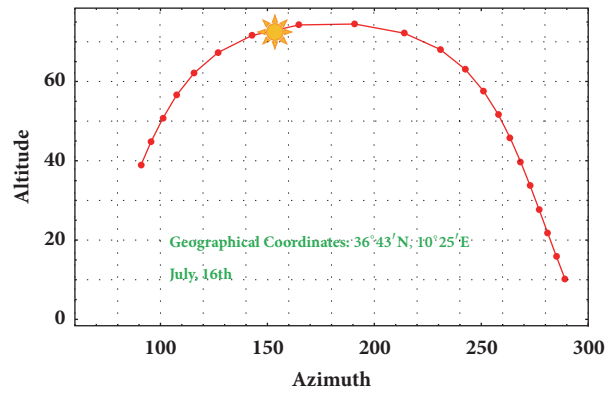

Figure 8: Solar chart for a typical summer day in Tunis-Tunisia (8:00–18:00 in 0:30 intervals).

COP_{cycle} = 0.84, 0.91, 0.95 for chilled water temperature, respectively, set at 7∘C, 10∘C, 12∘C, with corresponding values for COP_{system} = 0.51, 0.55, 0.58.

(iv) COP_{system} is 60% lower than COP_{cycle}. It ranges between 0.1 and 0.6, comparable with the results other authors [22, 23].

(v) When the cooling medium temperature is set at 32∘C, the performances of the cycle and the system reach their maximum at the highest pressure in the generator (270 kPa) and for a chilled water temperature T_c = 12∘C.

5.3. Case Study: Hourly Local Data. Belghouthi *et al.* [18] performed a thermal test of weather and solar conditions during July 2008 at a research centre in `Borj Cedria`, near Tunis. The research centre is located at 36°43' latitude and 10°25' longitude. Figure 7 shows the data for a particular day (16th of July 2008), of this Mediterranean climate zone characterized by a high level of solar resources. It receives an average of 17 kJ/m^2/day with a total insolation period of 3500 h/year and 350 sunny days per year. Ambient temperature varies between 39°C and 27°C, and solar radiation in the range 250 W/m^2–900 W/m^2. Maximum solar radiation of 958 W/m^2 is observed at 12:00. Maximum ambient temperature of 37°C is found at 14:00. Figure 8 reproduces the solar chart for the test day.

The efficiency of the Fresnel collector as expressed in (5) depends on the quadratic temperature difference $\Delta T = T_{HTF} - T_{amb}$ (equation (2)) between that of heat transfer flow and ambient. In the high-lightened gray interval in Figure 4, the temperature T_{HTF} affects more the collector efficiency than the irradiance G. Considering the model equations (1)-(5) and Figure 4, the lower is T_{HTF} the higher is the collector efficiency. Due to the compensating effects of solar radiation and ambient temperature during the time interval 11:00-15:00, the efficiency of the collector is at its maximum at this period as shown in Figures 9 and 10.

Figure 11 shows the evolution COP_{system} and COP_{cycle} during the test summer day. The COP_{cycle} reaches always values higher than 0.9 and the COP_{system} is higher than 0.55. The cycle performances are independent on ambient temperature, set at 25°C; this is the reason of the constant COP_{cycle}. The maximum COP_{system} is equal to 0.99, 1.02, 1.03 for generator pressure set, respectively, at 198 kPa, 232 kPa, and 270 kPa. The evolution of COP_{system} is similar to that of the collector efficiency; it reaches its maximum in the middle of the day from 12:00 to 14 pm, namely, 0.61, 0.63, and 0.63 for

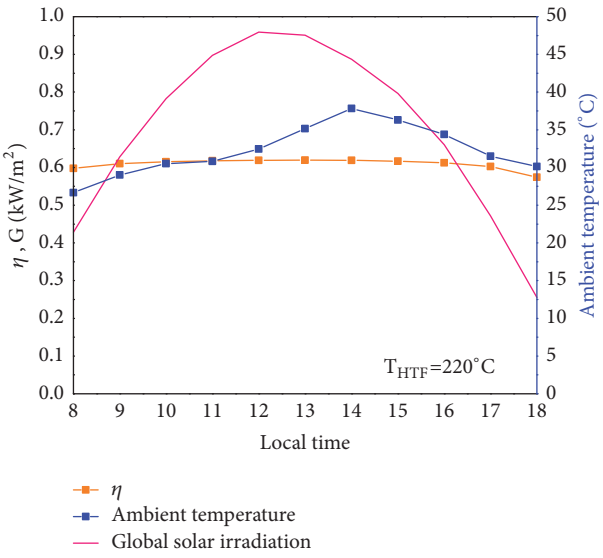

Figure 9: Collector efficiency *versus* ambient temperature and solar radiation for a fixed temperature T_{HTF} = 220°C and climate conditions of Figure 7.

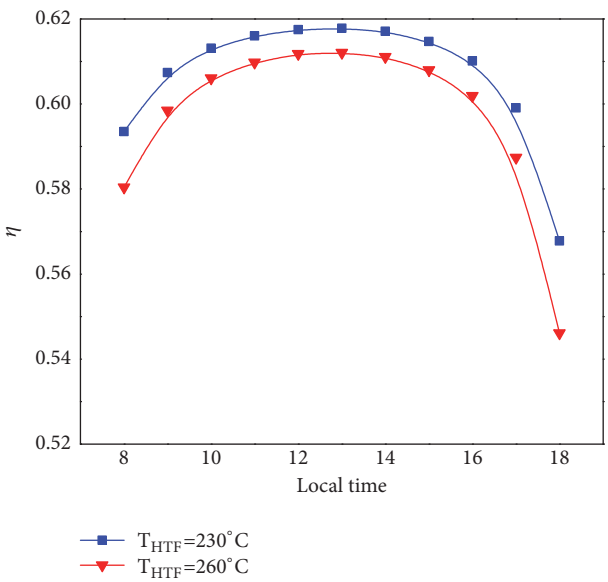

Figure 10: Collector efficiency during typical Tunisian summer day for different HTF temperatures.

generator pressure set, respectively, at 198 kPa, 232 kPa, and 270 kPa.

6. Conclusion

This paper investigated solar combined ejector single-effect absorption refrigeration cycle. The considered chiller is driven by condensation of steam at temperatures between 180°C and 210°C, using pressurized water heated by a linear Fresnel collector.

The model of the collector is detailed and simulations of the overall system and the cooling machine are performed.

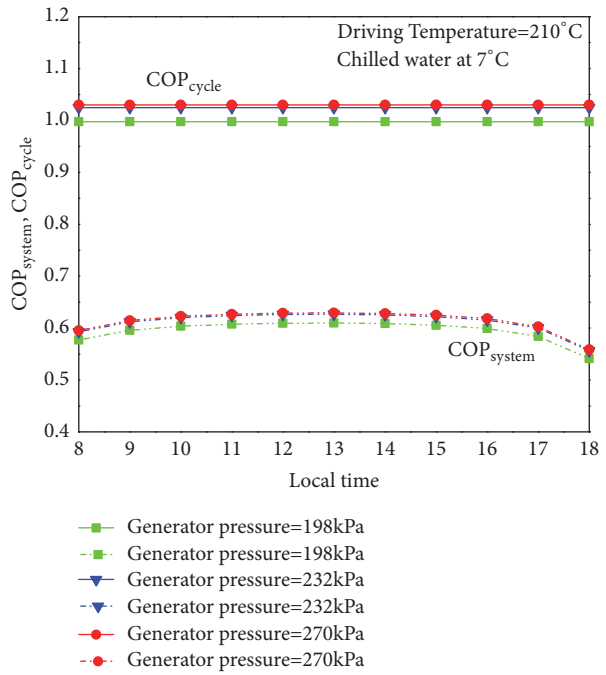

Figure 11: Hourly evolution of COP_{system} and COP_{cycle} during a typical Tunisian summer day for different generator pressure.

The produced water chilled water is varied between 7°C and 12°C. In regard to the simulation results, it can be concluded that

(i) The *COP* increases with the driving the heat temperature increases, decreases when cooling medium temperature gets higher, and increases with the chilled water temperature.

(ii) The COP_{cycle} of this particular single-effect cycle can reach 1.03, a value comparable to that of a conventional double-effect cycle.

(iii) For fixed cooling medium temperature, the maximum *COP* reaches higher values when the generator pressure is larger, *e.g.*, for a cooling medium set at 25∘C and solution generator temperature at 210∘C, the COP_{cycle} = 0.99, 1.02, 1.03 and the COP_{system} = 0.57, 0.59, 0.6, respectively, for generator pressure is at 198 kPa, 232 kPa, and 272 kPa.

(iv) COP_{system} is almost half of COP_{cycle} due to the limited efficiency of the solar collector compartment, between 0.5 and 0.6.

(v) For a fixed generator pressure, the maximum *COP* decreases when the temperature of the cooling medium rises. For a generator pressure of 198 kPa and chilled water temperature at 7∘C, the maximum COP_{cycle} is 0.99, 0.85, and 0.75 for cooling medium temperature of 25∘C, 30∘C, and 35∘C, respectively. The corresponding values of COP_{system} are 0.57, 0.52, and 0.46.

(vi) For a cooling medium temperature of 32∘C and by fixed chilled water temperature, the COP_{cycle} and the

COP_{system} increase with the driving heat temperature, reaching a maximum for $T_g = 210\circ$C: 0.87, 0.91, and 0.95 for, respectively, 198 kPa, 232 kPa, and 270 kPa generator pressure and at 12∘C chilled water temperature.

(vii) The performances of cycle and system are optimal for the highest generator pressure (270 kPa in this study) and chilled water temperature (12∘C).

A case study of a typical summer day is simulated; results showed that

(i) The average efficiency of linear Fresnel collector considered in the simulations varies between 0.6 and 0.62.

(ii) In the test period, COP_{cycle} reaches values always higher than 0.9 and COP_{system} larger than 0.55. The cycle performances are independent from ambient temperature with a maximum equal to 0.99, 1.02, and 1.03 for generator pressure, respectively, at 198 kPa, 232 kPa, and 270 kPa.

(iii) The system performance evolves parallel to that of the collector efficiency, reaching its maximum in the middle of the day from 12:00 to 14 pm.

Data Availability

Previously reported solar collector data used to support this study are available at [W. Christine, B. Michael, M. Florian, H. Alexander, N. Tomas, "Solar cooling with water-ammonia absorption chillers and concentrating solar collector-operational experience", International Journal of refrigeration, vol. 39, pp. 57-76, 2014.]. These prior studies and datasets are cited at relevant places within the text as [17]. Also the local metrological data were used to support this study and are available at [M. Balghouthi, M. H. Chahbani, and A. Guizani, "Investigation of a solar cooling installation in Tunisia," Applied Energy, vol. 98, pp. 138–148, 2012.]. These prior studies and datasets are cited at relevant places within the text as [18].

Conflicts of Interest

The authors declare that they have no conflicts of interest.

References

[1] K. Kaygusuz, "Prospect of concentrating solar power in Turkey: the sustainable future," *Renewable & Sustainable Energy Reviews*, vol. 15, no. 1, pp. 808–814, 2011.

[2] M. U. H. Joardder, P. K. Halder, A. Rahim, and N. Paul, "Solar Assisted Fast Pyrolysis: A Novel Approach of Renewable Energy Production," *Journal of Engineering*, vol. 2014, Article ID 252848, 10 pages, 2014.

[3] F. J. Cabrera, A. Fernández-García, R. M. P. Silva, and M. Pérez-García, "Use of parabolic trough solar collectors for solar refrigeration and air-conditioning applications," *Renewable & Sustainable Energy Reviews*, vol. 20, pp. 103–118, 2013.

[4] S. Beerbaum and G. Weinrebe, "Solar thermal power generation in India - A techno-economic analysis," *Journal of Renewable Energy*, vol. 21, no. 2, pp. 153–174, 2000.

[5] G. Manzolini, M. Bellarmino, E. Macchi, and P. Silva, "Solar thermodynamic plants for cogenerative industrial applications in southern Europe," *Journal of Renewable Energy*, vol. 36, no. 1, pp. 235–243, 2011.

[6] A. Maiorino and M. Valentini, "On the technical and economic feasibility of a solar thermodynamic power plant in an area of medium–high direct sunlight intensity: an actual case study," *Journal of the Brazilian Society of Mechanical Sciences and Engineering*, vol. 39, no. 1, pp. 245–257, 2016.

[7] K. Ajay and L. Kundan, "Combined Experimental and CFD Investigation of the Parabolic Shaped Solar Collector Utilizing Nanofluid (CuO-H2O and SiO2-H2O) as a Working Fluid," *Journal of Engineering*, vol. 2016, Article ID 5729576, 10 pages, 2016.

[8] O. Marc, G. Anies, F. Lucas, and J. Castaing-Lasvignottes, "Assessing performance and controlling operating conditions of a solar driven absorption chiller using simplified numerical models," *Solar Energy*, vol. 86, no. 9, pp. 2231–2239, 2012.

[9] G. A. Florides, S. A. Kalogirou, S. A. Tassou, and L. C. Wrobel, "Modelling and simulation of an absorption solar cooling system for Cyprus," *Solar Energy*, vol. 72, no. 1, pp. 43–51, 2002.

[10] G. A. Florides, S. A. Kalogirou, S. A. Tassou, and L. C. Wrobel, "Modelling, simulation and warming impact assessment of a domestic-size absorption solar cooling system," *Applied Thermal Engineering*, vol. 22, no. 12, pp. 1313–1325, 2002.

[11] A. Shirazi, R. A. Taylor, S. D. White, and G. L. Morrison, "Multi-effect absorption chillers powered by the sun: reality or a reverie," *Energy Procedia*, vol. 91, pp. 844–856, 2016.

[12] D. Chemisana, J. López-Villada, A. Coronas, J. I. Rosell, and C. Lodi, "Building integration of concentrating systems for solar cooling applications," *Applied Thermal Engineering*, vol. 50, no. 2, pp. 1472–1479, 2013.

[13] H. Beltagy, D. Semmar, C. Lehaut, and N. Said, "Theoretical and experimental performance analysis of a Fresnel type solar concentrator," *Journal of Renewable Energy*, vol. 101, pp. 782–793, 2017.

[14] P. Bermejo, F. J. Pino, and F. Rosa, "Solar absorption cooling plant in Seville," *Solar Energy*, vol. 84, no. 8, pp. 1503–1512, 2010.

[15] D.-W. Sun, I. W. Eames, and S. Aphornratana, "Evaluation of a novel combined ejector - Absorption refrigeration cycle - I: Computer simulation," *International Journal of Refrigeration*, vol. 19, no. 3, pp. 172–180, 1996.

[16] S. Aphornratana and I. W. Eames, "Experimental investigation of a combined ejector-absorption refrigerator," *International Journal of Energy Research*, vol. 22, pp. 195–207, 1998.

[17] C. Weber, M. Berger, F. Mehling, A. Heinrich, and T. Núñez, "Solar cooling with water-ammonia absorption chillers and concentrating solar collector - Operational experience," *International Journal of Refrigeration*, vol. 39, pp. 57–76, 2014.

[18] M. Balghouthi, M. H. Chahbani, and A. Guizani, "Investigation of a solar cooling installation in Tunisia," *Applied Energy*, vol. 98, pp. 138–148, 2012.

[19] T. Sriveerakul, S. Aphornratana, and K. Chunnanond, "Performance prediction of steam ejector using computational fluid dynamics: Part 1. Validation of the CFD results," *International Journal of Thermal Sciences*, vol. 46, no. 8, pp. 812–822, 2007.

[20] S. A. Klein and F. Alvarado, *Engineering equation solver*, F–chart software, Middletonm, Wis, USA.

[21] R. Fathi, C. Guemimi, and S. Ouaskit, "An irreversible thermodynamic model for solar absorption refrigerator," *Journal of Renewable Energy*, vol. 29, no. 8, pp. 1349–1365, 2004.

[22] R. Gomri, "Investigation of the potential of application of single effect and multiple effect absorption cooling systems," *Energy Conversion and Management*, vol. 51, no. 8, pp. 1629–1636, 2010.

[23] H. K. Ersoy, S. Yalcin, R. Yapici, and M. Ozgoren, "Performance of a solar ejector cooling-system in the southern region of Turkey," *Applied Energy*, vol. 84, no. 9, pp. 971–983, 2007.